Defence Research and Development Canada
Recherche et développement pour la défense Canada

DRDC | RDDC
technologysciencetechnologie

Design of new Frequency Modulated Continuous Wave (FMCW) target tracking radar with digital beamforming tracking

A Scientific Report on high fidelity radar electronic warfare modelling and simulation and hardware in-the-loop

Taiwen Tang
Chen Wu
DRDC – Ottawa Research Centre

Defence Research and Development Canada
Scientific Report
DRDC-RDDC-2019-R175
December 2019

Canada

IMPORTANT INFORMATIVE STATEMENTS

This document was reviewed for Controlled Goods by Defence Research and Development Canada (DRDC) using the Schedule to the *Defence Production Act*.

Endorsement statement: This publication has been peer-reviewed and published by the Editorial Office of Defence Research and Development Canada, an agency of the Department of National Defence of Canada. Inquiries can be sent to: Publications.DRDC-RDDC@drdc-rddc.gc.ca.

Abstract

Frequency modulated continuous wave (FMCW) radars have large time-bandwidth product factor with long detection range and accurate range resolution using low emitting power, which impose a great challenge for electronic support measure (ESM) systems to detect such radars. For better understanding of the radar technology and assisting radar electronic warfare (REW) research and development (R&D), this Scientific Report presents a new FMCW radar system design with a phased array and digital beamforming (DBF) for monopulse multi-target tracking. The radar computer model can also be used in radio frequency (RF) high-fidelity modelling and simulation (M&S) for REW studies. A number of design challenges are addressed in the report, including the use of 1) Chebyshev window and digital notch filter to overcome the transmitter-to-receiver leakage in the radar, 2) DBF for simultaneously multi-target tracking, and 3) feedback control loop design. Using a digital filter, this report also introduces a new RF M&S scheme that addresses the continuous target movement modeled in the sampled signal domain. This scheme provides a general approach that allows the digital/time-based RF M&S to incorporate the analog signals at any required time instant without increasing the time sampling rate.

Significance to defence and security

In Air RF warfare (03dc) project, an RF high-fidelity modelling and simulation—hardware-in-the-loop (RF M&S-HWIL) capability is being developed. The capability has been used to support Royal Canadian Air Force (RCAF) RF electronic warfare (EW) test and evaluation, and also applied for advanced REW R&D. This Scientific Report is one of research reports of the project.

Modern frequency modulated continuous wave (FMCW) radars have large time-bandwidth product factor and can offer long detection range and accurate range resolution with low emitting power, which imposes a great challenge for REW system to detect such low power radars. Using RF high-fidelity M&S method, a new FMCW radar system with digital phased-array technology is presented in this report. The research result allows the REW researchers 1) having an good opportunity to better understand such modern radar technology, 2) using the radar computer model in RF high-fidelity M&S for REW studies, 3) implementing the radar signal processing algorithms in field programmable gate array for HWIL tests in the near future, and 4) supporting the development of electronic support measures and countermeasures techniques in REW R&D.

Résumé

Les radars à onde continue modulée en fréquence (OCMF) ont un facteur produit durée-bande passante élevé, une grande portée de détection et une résolution en portée précise, malgré leur faible puissance d'émission. Cela complique grandement la détection par les systèmes de mesure de soutien électronique (MSE). Dans le but de mieux comprendre cette technologie radar et de soutenir les efforts de recherche et développement (R&D) en guerre électronique par radar (GER), le présent rapport scientifique contient la description d'un nouveau concept de système radar OCMF à balayage électronique et mise en forme numérique du faisceau pour la poursuite multicibles monoimpulsion. Le modèle informatique de radar présenté peut aussi servir en modélisation et simulation RF à haute fidélité pour les recherches en GER. Le rapport traite d'un certain nombre de difficultés de conception rencontrées, notamment l'utilisation 1) de la fenêtre de Tchébychev et d'un filtre numérique à coupure brusque pour éviter les pertes à la terre entre l'émetteur et le récepteur du radar; 2) de mise en forme numérique du faisceau pour la poursuite multicibles; et 3) d'une conception fondée sur une boucle de réaction. Le rapport présente aussi une nouvelle méthode de modélisation et simulation RF par filtrage numérique qui tient compte du mouvement continu des cibles modélisé dans le domaine des signaux échantillonnés. Il s'agit d'une technique générale qui permet à la modélisation et la simulation RF (temporelle ou numérique) d'intégrer des signaux analogiques au moment voulu sans devoir augmenter le taux d'échantillonnage.

Importance pour la défense et la sécurité

Dans le cadre du projet de guerre aérienne par RF (03dc), on est à mettre au point une capacité de modélisation et simulation RF à haute fidélité—matériel incorporé (RF M&S-HWIL). On utilise celle-ci pour appuyer l'évaluation et l'essai de guerre électronique (GE) par RF de l'Aviation royale canadienne (ARC). On l'emploie également pour la recherche et développement (R&D) en matière de GE par radar (GER) évoluée. Le présent document constitue l'un des rapports de recherche de ce projet.

Les radars à onde continue modulée en fréquence (OCMF) ont un facteur produit durée-bande passante élevé, une grande portée de détection et une résolution en portée précise, malgré leur faible puissance d'émission. Cela complique grandement la détection par les systèmes de mesure de soutien électronique (MSE). Le document présente un nouveau concept de système radar OCMF à balayage électronique qui exploite la modélisation et la simulation RF à haute fidélité. Les résultats de ces recherches aideront les chercheurs en GER, car 1) c'est une excellente occasion d'approfondir leurs connaissances de ces systèmes radar modernes, 2) ils pourront utiliser le modèle radar mis au point par modélisation et simulation RF à haute fidélité pour leurs recherches en GER, 3) les algorithmes de traitement des signaux radar seront bientôt intégrés aux matrices prédiffusées programmables par l'utilisateur (FPGA) pour les essais de matériel incorporé, et 4) ces recherches viennent appuyer la mise au point de mesures et de contre-mesures de soutien électronique en R&D pour la GER.

Table of contents

List of figures

List of tables

Acknowledgements

The authors would like to acknowledge Mr. Janaka Elangage for the insightful comments.

This page intentionally left blank.

1 Introduction

Low probability intercept radars (LPI) [1],[2] impose a great challenge to radar electronic warfare (REW) systems in detection and counter measuring them. Among those modern radar design technologies, the frequency modulated continuous wave (FMCW) waveform is often used in LPI radar designs, since it has large time-bandwidth product, and can offer long range detection with accurate range resolution using low emitting power. In order to develop electronic support measures (ESM) and electronic countermeasures (ECM) techniques in REW to deal with FMCW-based radars, solid understanding of such radar system is import for REW researchers.

The main objective of this research in the Air RF Warfare (03dc) project is to develop an FMCW radar system in hardware that can be used in the open-air trials to test the ESM and ECM systems and other REW techniques. This report presents the first step of this development that is the FMCW system design using Matlab/Simulink software. The radar system computer model in the Matlab/Simulink will also be used in the RF high-fidelity modelling and simulation (M&S) for computer based REW studies. The radar system signal processing algorithms will be put into field programmable gate array (FPGA) for hardware implantation used in the lab-based RF M&S-HWIL (hardware-in-the-loop) REW studies, which include developing ECM methods in jamming and the radar electronic counter-countermeasures (ECCM) methods. The ECM and ECCM studies on this FMCW radar will be presented in another report.

This report is organized as follows. Section 2 gives the FMCW radar system overview, and how it is modeled in the Matlab/Simulink. Section 3 discusses the considerations of the radar system transmitter (TX). The radar receiver (RX) antennas with detailed digital phase array (DPA) and digital beamforming (DBF) design are discussed in Section 4. In this section, we also 1) discuss the TX-to-RX coupling (or leaking) and how to apply a window function and a digital notch filter to reduce the coupling, and 2) address how to incorporate continuously changing analog signals, e.g., the continuous movement of a target location, into Matlab/Simulink digital-based M&S. Section 5 specifies the RF frontend and discusses some simulation parameter assumptions. Section 6 gives radar system simulation results. The conclusions can be found in the last section.

2 The FMCW radar system overview

The high level FMCW radar system is illustrated in Figure 1. The radar is mainly used as a target tracking radar (TTR). The radar system consists of a RX and a TX. The RX is a DPA receiving system formed by a $M \times N$ element phased array and the same number of RF receivers. Each antenna and its connected RF receiver will be called a receiving channel. The TX mainly has a FMCW signal generator, a RF power amplifier and an antenna radiation system. There are about three TX radiating antenna architectures in the modern TTR systems that use a DPA. The first one is a highly directional TX antenna. A good scheduling scheme is required in order to closely work with the DPA to track targets. The second method is the TX antenna which is a multi-beam antenna system to pair with DPA to track multiple targets. The third one is the TX antenna which has a sector antenna beam, as shown in Figure 1, that covers a portion of 3D space to illumine targets in the sector continuously. Although the first TX radiation system has high gain with simply antenna design, it cannot track its targets continuously and needs a good scheduling algorithm to point the antenna to target directions sequentially. The second approach can continuously track a number of targets with good antenna gain of each beam, the cost of such radiation system can be very high. The antenna gain of the radiation system in the last approach can be much lower than those in the first two approaches, but the antenna can be very simple and to achieve continuous target tracking. In addition, it also reduces the target search requirement. The sector TX antenna approach is used in this FMCW TTR design. Other TX antenna methods will be studied in future reports.

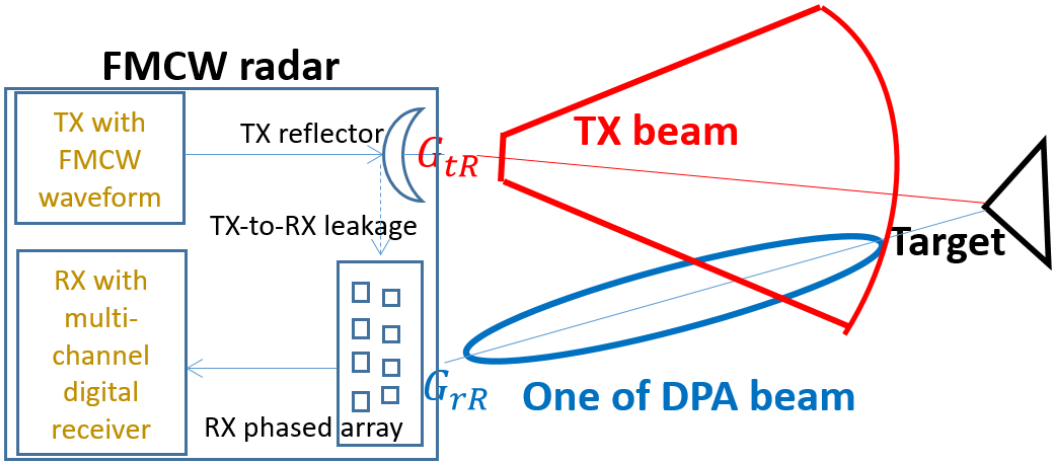

Figure 1: *High level FMCW radar block diagram and one of the radar tracked targets.*

In Figure 1, one of the targets in the TX sector antenna beam is illustrated in the far distance from the FMCW radar. It is assumed that 1) the target is a point reflecting source, and is modeled by its radar cross section (RCS) (σ), 2) the antenna gains of the TX and RX in the direction of the target are G_{tR} and G_{rR}, respectively.

Note that, the radar system has separated TX and RX antennas. It operates in the bi-static mode. The distance between the phase reference centers of these antennas is d_{TR}, which is assumed much smaller than the distances between the radar and its targets. One of the design challenge is the electromagnetic coupling between the TX and RX antennas, which is also known as TX-to-RX leakage, as shown in the figure. A digital notch-filter is used to reduce this coupling. The assumption that d_{TR} is much smaller

than the target range is very important in order to allow the filter working properly. More details of the de-coupling method will be discussed in Section 4.

As mentioned in Section 1, Matlab/Simulink software was used to model and design the radar and the scenario shown in Figure 1. Since the design focused on the digital baseband (BB) signal processing without modelling the details of RF analog systems in TX and RX, the radar equation model was used to model the radar received power, as a function of the distance between the radar and its target RCSs. The equation is

$$P_r = P_t + G_{tR} + G_{rR} + \sigma + 10 * \log_{10}\left(\frac{\lambda^2}{(4\pi)^3 R^4}\right) - L \tag{1}$$

where P_r is the received signal power in dBm, P_t is the transmitted signal power in dBm, G_{tR} is the transmit antenna gain of the radar in dBi, G_{rR} is the receive antenna gain of the radar in dBi, σ is in dBm^2, λ is the wavelength of the carrier frequency, R is the distance between the radar and the target in meters, which is much bigger than d_{TR}, and L is the loss in dB. Note that, since the targets move, all the parameters in (1) can change with time.

3 TX of FMCW radar and time domain modelling

3.1 TX subsystem of FMCW TTR

The TX Matlab/Simulink model of the FMCW TTR has a signal generator, a RF power amplifier and a sector antenna. The antenna is model by the antenna gain G_{tR}, and it covers the space that has one of targets in (ϕ, θ) direction, as shown in Figure 3. The RF power amplifier is modeled by a gain factor included in the P_t. In this section, we focus on the FMCW chirp signal.

3.2 FMCW radar chirp waveform

The uniqueness of an FMCW radar is its chirp waveform. In our radar design, a simple sawtooth chirp waveform [3] is used. Figure 2 shows an example of the time-frequency relationship in the signal. The signal frequency increases and upbeats linearly in each chirp with respect to the time increase. The signal can be expressed in the following equation:

$$x(t) = e^{2\pi jbt^2} \tag{2}$$

where b stands for the slope of the chirp, t is time, and the signal amplitude is equal to one. (2) can also be written in in- and quadrature-components (I/Q), when it is processed in the BB signal:

$$x(t) = x_I(t) + jx_Q(t) = \cos(2\pi bt^2) + j\sin(2\pi bt^2). \tag{3}$$

It is important to note that if the complex chirp waveform is delayed by τ, a frequency shift of $-2b\tau$ will appear in the delayed signal. This is the key feature that an FMCW radar obtains a target distance by measuring the frequency shift of the returned BB signal ($y(t)$) from its target. This feature can be shown in the following formula:

$$y(t) = e^{2\pi jb(t-\tau)(t-\tau)} = x(t)e^{2\pi jb\tau^2} \cdot e^{2\pi j(-2b\tau)t}. \tag{4}$$

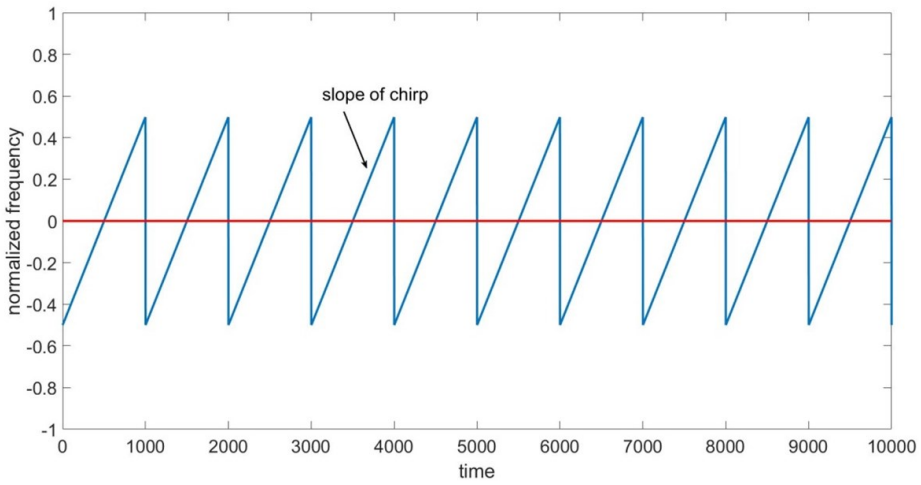

Figure 2: *Sawtooth shape of the chirp signal in time- and frequency-domain.*

From (4), the delayed version of the chip signal is changed by the factor of $e^{2\pi jb\tau^2}$ in its phase and down-shifts the frequency by the amount of $-2b\tau$.

3.3 Time-bandwidth product of the FMCW signal and LPI from ESM perspective

In [4], the FMCW time-bandwidth product is explained by an example. If the bandwidth is 10 MHz, and the sweep time is 1 ms (namely the FFT window duration that will be explained in Section 4), the time-bandwidth product is 10,000. Comparing a pulse-Doppler radar of the same power amplifier, 10 MHz bandwidth and 1 μs, the FMCW radar time-bandwidth product is 1,000 times larger. This implies 30 dB gain in digital signal processing for the FMCW radar vs. the pulse-Doppler radar.

In [4], the PILOT FMCW radar is given as an example about how it can achieve LPI. The PILOT radar operates at 9.375 GHz, with 30 dBi antenna gain, 1 W TX power, 3 dB noise figure and 1 ms sweep time. It can detect a target of 100 m^2 at 17 km distance. The ESM, however, can detect the radar signal at 2.5 km with 0 dBi antenna gain and -60 dBm minimum detectable power. The PILOT FMCW radar is therefore tactically undetectable by the ESM.

3.4 Time domain modelling of over-the-air propagation

In the TX, the complex BB chirp waveform $x(t)$ in (3) is up-converted to a carrier frequency f_c, the signal at the carrier frequency can be represented by a real signal

$$s(t) = \cos(2\pi(f_c + bt)t) \tag{5}$$

When this RF signal hits a moving target with the radial speed $v(t)$ (m/s) at a distance R_o, and bounces back to the radar receiver, the received signal can be expressed as:

$$r(t) = g * \cos\left(2\pi\left(f_c + b\left(t - \frac{2R(t)}{c}\right)\right)\left(t - \frac{2R(t)}{c}\right) + \varphi\right) \quad (6)$$

where g and φ are the gain and phase introduced by the electromagnetic (EM) wave reflection and other losses in the two-way path between TX and RX antennas respectively, and

$$R(t) = R_0 + \int_0^t v\,(\tau)d\tau \quad (7)$$

where $R(t)$ is the distance between the Radar and the target. In this research, it is assumed that the RF propagation channel between the TX antenna and each receiving antenna element in the phased array has all-pass characteristics. This assumption implies that the receiving phased array is calibrated to remove all the differences of extra delays, the gains and phases of the RF paths among $M \times N$ receiving channels.

4 RX part of the FMCW radar

4.1 Introduction

The DPA technology is used in the FMCW TTR design with advanced digital signal processing (DSP) methods. Each part of the processing chain in the RX system will be discussed in this section. We start with the phased array antenna. After that, following the received signal path in the RX, we present the digital signal processing algorithms used to process the complex BB signals. Finally, we discuss how to use digital filters to model continuous target delays of complex BB signals in the digital domain.

4.2 Radar RX antenna coordinate system

The coordinate system used in the M&S is presented in Figure 3. The panel of the RX phased array is in the XZ-plane, and its phase reference center is at the origin of the Cartesian coordinate. A target is located at (ϕ, θ, R), which is also known as azimuth-angle (Az) (in degree), elevation-angel (El) (in degree) and range (R) (in meter). Since the target moves, the (ϕ, θ, R) changes continuously with time.

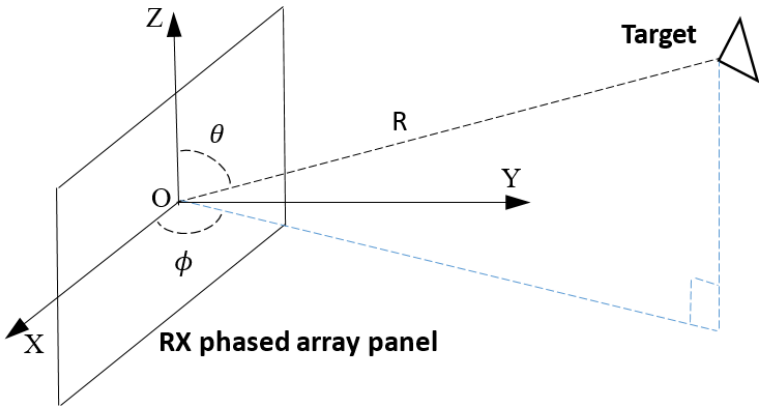

Figure 3: *RX phased array panel and target.*

4.3 $M \times N$ element phased array

It is assumed that the phased array has M and N elements in X- and Z-direction, respectively, as shown in Figure 4. In our design, the array has a uniform element spacing (d_c) in both X- and Z-directions. Without loss of generality, it is also assumed M and N are even numbers. Based on the microwave antenna array theory, the array factor in the direction of (ϕ, θ) can be written as, if all the elements are uniformly excited with unit amplitude:

$$AF_{ik}(\phi, \theta) = e^{-j\,\vec{\boldsymbol{K}}(\phi,\theta)\cdot\vec{\boldsymbol{R}}(i,k)} \tag{8}$$

where $\vec{\boldsymbol{K}}(\phi, \theta)$ is the wavenumber in the direction of (ϕ, θ), and $\vec{\boldsymbol{R}}(i, k)$ is the displacement from the $(i, k)^{th}$ element to the target in (ϕ, θ) direction, they can be expressed as

$$\vec{\boldsymbol{K}}(\phi,\theta) = \frac{2\pi}{\lambda}\{\cos(\phi)\sin(\theta)\,\hat{\boldsymbol{x}},\quad \sin(\phi)\sin(\theta)\,\hat{\boldsymbol{y}},\quad \cos(\theta)\,\hat{\boldsymbol{z}}\} \tag{9}$$

where λ is the free space wavelength, and

$$\vec{\boldsymbol{R}}(i,k) = \{x(i)\,\hat{\boldsymbol{x}},\quad 0\,\hat{\boldsymbol{y}}, z(k)\hat{\boldsymbol{z}}\} \tag{10}$$

since the array is in the XZ-plane, where $x(i) = d_c\left(i - \frac{M}{2} + 0.5\right)$ and $z(k) = d_c\left(k - \frac{N}{2} + 0.5\right)$. The vector $\hat{\boldsymbol{x}}, \hat{\boldsymbol{y}}$ and $\hat{\boldsymbol{z}}$ are unit vectors on x, y and z axis**.** So that (8) can be rewritten as

$$AF_{ik}(\phi,\theta) = e^{-j2\pi\frac{d_c}{\lambda}\left(a(1)\cdot\left(i-\frac{M}{2}+0.5\right)+a(2)\cdot\left(k-\frac{N}{2}+0.5\right)\right)} \tag{11}$$

where

$$[a(1), a(2)] = [\cos(\phi)\sin(\theta),\ \cos(\theta)]. \tag{12}$$

The term of $\left[2\pi\,\frac{d_c}{\lambda}\left(a(1)\cdot\left(i-\frac{M}{2}+0.5\right)+a(2)\cdot\left(k-\frac{N}{2}+0.5\right)\right)\right]$ in (11) can also be considered as the phase needed on $(i,k)^{\text{th}}$ element in order to let the array form a beam in (ϕ,θ) direction.

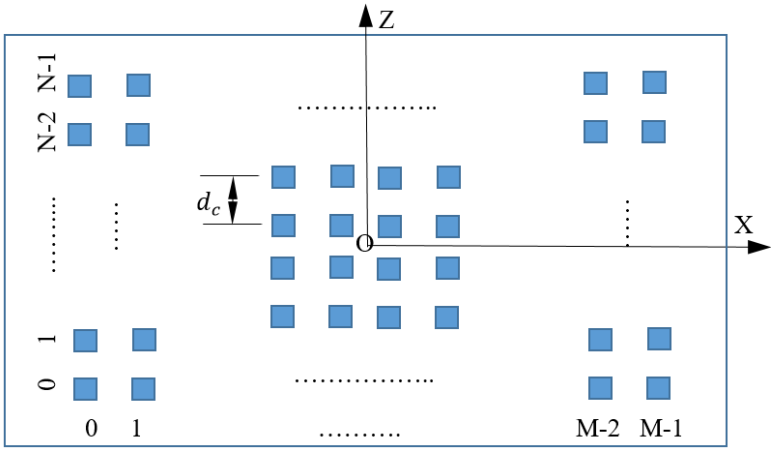

Figure 4: *Element locations of the phased array in XZ-plane.*

We define the beamforming coefficient of the $(i,k)^{\text{th}}$ element in the array as

$$b_{ik}^{c} = e^{j2\pi\frac{d_c}{\lambda}\left(a(1)\cdot\left(i-\frac{M}{2}+0.5\right)+a(2)\cdot\left(k-\frac{N}{2}+0.5\right)\right)} \tag{13}$$

4.4 Received signal

After the two-way propagation, the target echo signal $r(t)$ is intercepted by the elements in the RX phased array. At the $(i,k)^{\text{th}}$ element the received analog signal in the complex format can be expressed as

$$r_{ik}(t) = g_{ik}^{c} \cdot e^{2\pi j\left(-\frac{2f_c R(t)}{c}\right)} \cdot x\left(t - \frac{2R(t)}{c}\right) \tag{14}$$

where g_{ik}^{c} is the complex gain coefficient of the $(i,k)^{\text{th}}$ element.

The received signal then is down-converted by the RF front-end, and digitized by an ADC (analog to digital converter) sampling at the rate of f_S, the sampled signal is

$$r_{ik}[n] = g_{ik}^{c} \cdot e^{2\pi j\left(-\frac{2f_c R(nT_S)}{c}\right)} \cdot x\left(nT_S - \frac{2R(nT_S)}{c}\right) \tag{15}$$

where n is the n^{th} time sample step, $T_S = 1/f_S$. the complex gain coefficient can be rewritten as

$$g_{ik}^{c} = \sigma \cdot g^{air} \cdot AF_{ik}(\phi,\theta) \cdot h_{rf}^{c} \tag{16}$$

where σ is the target RCS, g^{air} is the propagation loss defined by the radar equation in (1), h_{rf}^{c} is the RX RF channel gain, and the array factor $AF_{ik}(\phi,\theta)$ is in (13).

4.5 Block diagram of the DSP

Figure 5 illustrates the signal flow in the RX system. The complex I/Q samples (right side of the figure) from ADCs are first sent to five digital beamforming (DBF) boxes. Next de-chirping and notch filtering are applied to the five DBF signals. The notch filter is used to remove the DC portion of the TX-to-RX leakage. This makes the desired tone detection simpler if the desired tone is close to DC. Then five signals are fed to the windowed FFT and desired tone detection block. We use a digital control loop to track the angles and perform beamforming. The loop contains two decoupled PI controllers in the feedback path. The PI controller utilizes the error signals to generate the angle information for the digital beam forming. We apply a Chebyshev window of $120\ dB$ sidelobe suppression before taking FFT. The Chebyshev window is intended to remove the sidelobes of the strong DC spur caused by the continuous digital beamforming.

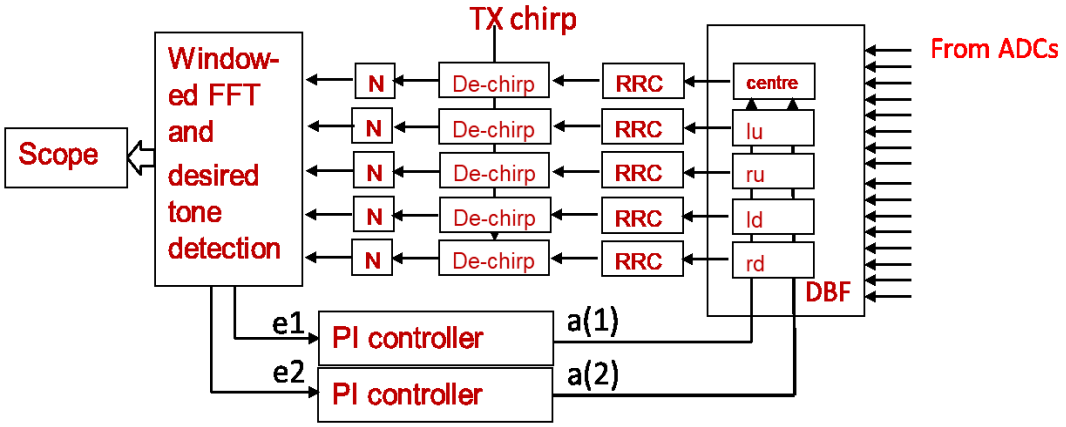

Figure 5: *The digital signal processing diagram of the radar system. RRC is the root-raised-cosine filter. De-chirp is the de-chirp operation, N means notch filtering processing, DBF is digital beamforming.*

4.6 Monopulse radar tracking and five digitally formed beams

In the monopulse angle-tracking, the receiving antenna has four apertures A, B, C and D as shown in Figure 6 (left). These apertures form five antenna beams in the space (Figure 6 (right)). The sum-beam (centre) is obtained by adding the signals of all antenna elements after applying the digital beamforming. The approach of using five beams is called amplitude monopulse method. The beamforming process of these five beams are described in Equations (17)–(20). If the energies collected in these beams are named as $p_{lu}, p_{ru}, p_{ld}, p_{rd}$ in the dB scale, the elevation tracking intends to adjust the antenna direction to make $p_{lu} + p_{ru} = p_{ld} + p_{rd}$ and the azimuth tracking intends to make $p_{ld} + p_{lu} = p_{rd} + p_{ru}$ [5]. The feedback part of the tracker can be PID (proportional-integral-derivative) controllers. The second angle tracking method utilizes the phase information in four beams. The differential phase information between signals of A + B and C + D, and signals of A + C and B + D are used to form the elevation and azimuth tracker, respectively. The trackers intend to alter the antenna direction in order to drive the differential angles to zeroes, i.e., to make Az- and El-boresight directions matching the target direction (ϕ, θ).

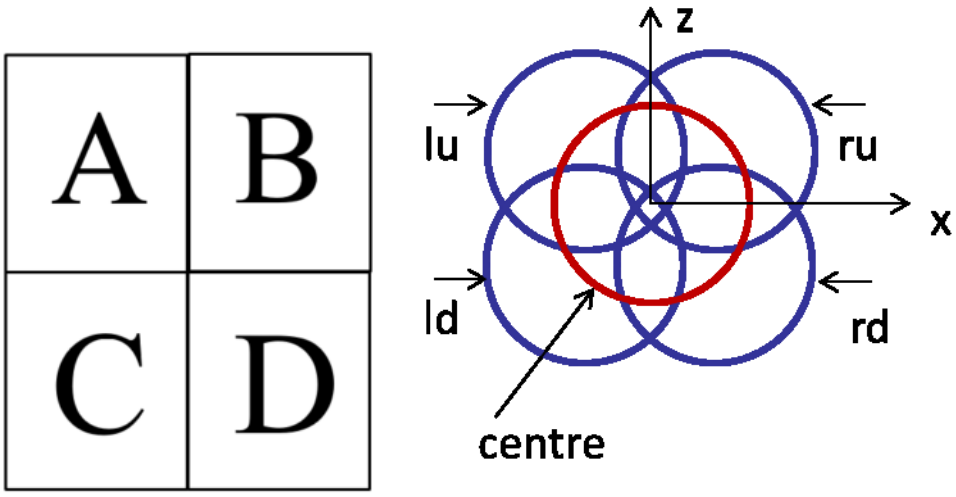

Figure 6: *Four apertures on the antenna plane (left) and five antenna beams (right) in the space, note that the view direction is from radar to target, i.e., Y-direction points into the paper.*

If the sum-beam points to the target direction (ϕ, θ), the tracking direction is defined by (12). Then other four beam directions can be expressed as

$$\begin{aligned} a_{lu} &= [\cos(\phi)\sin(\theta) + \delta, \quad \cos(\theta) - \delta] \\ a_{ru} &= [\cos(\phi)\sin(\theta) - \delta, \quad \cos(\theta) - \delta] \\ a_{ld} &= [\cos(\phi)\sin(\theta) + \delta, \quad \cos(\theta) + \delta] \\ a_{rd} &= [\cos(\phi)\sin(\theta) - \delta, \quad \cos(\theta) + \delta] \end{aligned} \tag{17}$$

where a_{lu}, a_{ru}, a_{ld} and a_{rd} represent the lu, ru, ld, rd beam directions, respectively, and δ indicates that these beam directions are a little away from the sum beam direction. Considering the array factor discussed in previous section, the amount digital phase shift applied to the $(i,k)^{\text{th}}$ element in the phased array in order to form a beam in the direction of pq (where $p = l$ or r and $q = d$ or u)

$$\alpha_{ik,pq} = 2\pi \frac{d_c}{\lambda}\left(a_{pq}(1)\cdot\left(i - \frac{M}{2} + 0.5\right) + a_{pq}(2)\cdot\left(k - \frac{N}{2} + 0.5\right)\right) \tag{18}$$

and amount digital phase shift of the $(i,k)^{\text{th}}$ element for the sum beam is

$$\alpha_{ik} = 2\pi \frac{d_c}{\lambda}\left(a(1)\cdot\left(i - \frac{M}{2} + 0.5\right) + a(2)\cdot\left(k - \frac{N}{2} + 0.5\right)\right) \tag{19}$$

Clearly, we can obtain the following signal after the beamforming operations:

$$y_{pq}[n] = \sum_i \sum_k r_{ik}[n] e^{j\alpha_{ik,pq}}$$
$$y[n] = \sum_i \sum_k r_{ik}[n] e^{j\alpha_{ik}}. \quad (20)$$

where $y_{pq}[n]$ and $y[n]$ are the signals of the lu, ru, ld, rd beams and the sum-beam.

4.7 De-chirp of DBF signals

Using the sum-beam signal as an example, here we discuss the de-chirp processing. The digital version of the transmitted chirp signal from (2) is written as $x[n]$. The output signal from de-chirp signal processing can be expressed as follows:

$$y_d[n] = x^*[n] \cdot y[n] \quad (21)$$

where $()^*$ is the complex conjugate operation.

As explained in Equation (4), a propagation delay in the roundtrip path of the waveform is translated to a negative frequency shift from the centre frequency. By analyzing the de-chirped signal $y_d[n]$ in the baseband, we can see a distinct frequency component, away from the origin of the frequency. The amount of frequency shift is in proportion to the signal delay.

4.8 Notch filter to reduce TX-to-RX leakage

Our FMCW radar uses separate TX and RX antenna systems, which can improve the isolation between the TX and RX antennas. However, as the target echo signal is very weak, more reduction of the coupling between TX and RX antennas is required. The reflected-power canceller method has been widely used in radar design [6],[7]. Since this method needs to use variable analog phase shifters in the RF analog signal path, it complicates the digital phased array RX antenna in our design. It is very difficult to identify a near DC tone caused by the useful target skin return and the TX-to-RX leakage. To mitigate this problem, a notch filter in the digital domain is applied to the signal after the de-chirp operation. The notch filter is

$$H(z) = \frac{(1 - z^{-1})^4}{(1 - 0.975z^{-1})^4} \quad (22)$$

The filter only works when the target range is much greater than the distance between TX and RX antennas. The filter design is discussed in Annex B. This filter can cancel the DC frequency component by more than 80 dB, and has less than 10 dB gain reduction when the normalized frequency is bigger than 0.005.

For a one-way propagation delay τ to be detectable in the digital domain after de-chirping, based on Equation (4) and Equation (21), it needs to satisfy the following inequality:

$$2\tau * 2b * T_B < 1, \tag{23}$$

where $T_B = \frac{1}{f_B}$ and f_B is the baseband sampling frequency. In the digital domain, phase wrap-around happens if the one-way propagation delay $\tau \geq \frac{0.25 f_B}{b}$. The distance $= \frac{0.25 f_B c}{b}$ is the wrap-around range of the radar, where c is the speed of light. When a tone appears at the normalized frequency $= 0.005$, the corresponding distance $= \frac{0.005c}{4bT_B}$. The design of the notch filter implies when the target range is bigger than 0.5% of the wrap-around range of the radar, there is a less than $10\,dB$ compromise to the gain of target signal as shown in Annex B.

4.9 Angle tracking error signals

In order to obtain the target echo signal power levels in the lu, ru, ld, rd beams, a simple FFT based signal separation is applied to consecutive N_{FFT} samples of $y_d[n]$ or $y_{d_{pq}}[n]$ given in (21). Each de-chirp signal energy can be estimated from the peak value at the FFT output, denoted by p_{pq} in dB, the angle-tracking errors can be formed as $e_1$and e_2 as shown here

$$e_1 = (p_{lu} + p_{ld}) - (p_{ru} + p_{rd}) \tag{24}$$

$$e_2 = (p_{ld} + p_{rd}) - (p_{lu} + p_{ru}) \tag{25}$$

for Az- and El-angle tracking, respectively. Using dB gain can significantly reduce the dynamic range of the error signal than using linear gain. This makes the control process converge to the correct equilibrium state with not too small value of c_1 in the PI controller (c_1 is similar to the convergence step size). Using a linear gain, we must use an extremely small value of c_1 in the PI controller and convergence time can be too long.

The tracking algorithm uses a PID controller in this design. It is very similar to the mono-pulse tracking. However, the key difference is the coherent combining via phase shifting and signal power detection in the post FFT domain. The peak values of the FFT have both amplitude and phase information. It can improve the anti-jamming tracking ability of the radar system, which will be reported in another report.

To make the angle tracking works for different ranges, a scaling factor that is inversely proportional to the estimated propagation delay is used to scale the error signal. The main rationale is that when the distance between the radar and the target is close, the angle tracking requires a big step size. Thus (24) and (25) become

$$e_1 = \frac{(p_{lu} + p_{ld}) - (p_{ru} + p_{rd})}{\mathrm{R/c}} \tag{26}$$

$$e_2 = \frac{(p_{ld} + p_{rd}) - (p_{lu} + p_{ru})}{\mathrm{R/c}} \tag{27}$$

4.10 Angle tracking loop design

The feedback part of the tracking loop design is the classical PI (proportional-integral) controller illustrated in Figure 7. The input to the tracking loop is the error signal ($e1\ or\ e2$), and the output is the tracking quantities $a(1)\ or\ a(2)$, corresponding to $\cos(\phi)\sin(\theta)$ or $\cos(\theta)$.

The PI controller can achieve an equilibrium state when the error signal ($e1\ or\ e2$) = 0. At this equilibrium state, the tracking quantities $a(1)$ and $a(2)$ converge statistically to the true beamforming angle quantities $cos(\phi)\sin(\theta)$ and $cos(\theta)$. The error signal needs to contain the information about the angle quantities, e.g., nonlinear representation of the angle quantities. We choose the power difference in dB in Az or El as the error signal, which is a nonlinear representation of the angle quantities. In this way, the PI loop is driven to achieve the equilibrium state in a nonlinear fashion. Since the solution is not closed form, we cannot derive the system transfer function. However, we can derive the transfer function for simple linear control problems. We illustrate how the PI loop works by looking a similar linear control problem shown in Figure 8.

The PI controller uses two discrete memory units. The loop parameters are $c1$ and $c2$. The controller can be described by the following response:

$$H_{PI}(z) = \frac{\left(c1 + \frac{c1c2}{1 - z^{-1}}\right)}{1 - z^{-1}}. \tag{28}$$

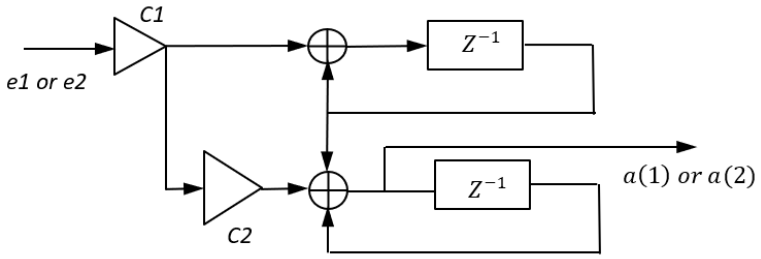

Figure 7: *PI controller. Input is the error signal and output is the estimate of tracking quantities.*

The beamforming angle tracking loop in Figure 5 can be described in a high level conceptual picture in Figure 8, however, these two block diagrams are not equivalent. The digital beamforming module in Figure 5 has similar characteristics as the subtraction operation in Figure 8 because the digital beamforming module matches the angle of arrivals of the input signal. This loop response according to Figure 8 is given as:

$$H_{loop}(z) = \frac{H_{PI}(z)}{1 + H_{PI}(z)}. \tag{29}$$

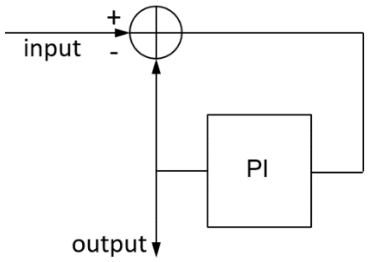

Figure 8: *High level diagram of the beamforming angle tracking loop. The subtraction operation is similar to the DBF operation in Figure 5.*

As an example, for $c1 = 0.03, c2 = \frac{1}{64}$, the loop filter response is shown in Figure 9. One can see that only DC component is retained with this loop structure. When compared with a feedforward implementation with a moving average filter of the form $H_{mavg}(z) = \frac{1}{64}\sum_{k=0}^{k=63} z^{-k}$, the PI loop achieves a similar loop response with a much lower complexity.

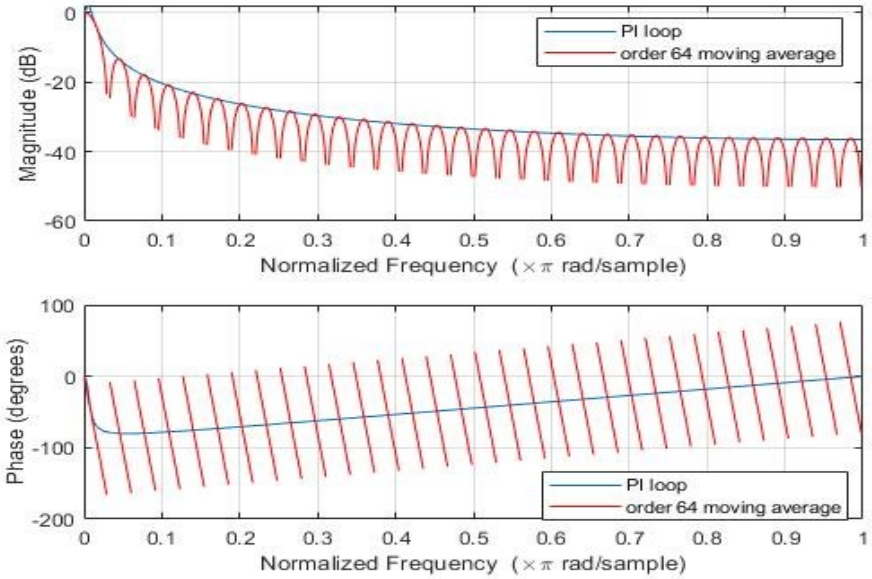

Figure 9: *PI control loop filter response.*

4.11 Desired tone detection

At the FFT output of the sum-beam signal, each peak has its unique characteristics. Some may represent the intended target signals, some may represent the remaining TX-to-RX leakage, and others may represent the jamming signal. The first step is to reliably detect the desired tones. We apply the following rule for the desired tone detection:

- Rule 1: If a local peak at the k^{th} frequency index is the maximum in the frequency proximity of $[k - p_{prox}, k + p_{prox}]$ at the FFT output, where p_{prox} is the frequency proximity range (a design parameter), a local peak/desired tone is claimed.

After DC notch filtering, there are still some peaks near DC in the negative and the positive frequencies. These peaks are caused by the fact that when the chirp signal sweeps across the baseband, the chirp signal's gain is also modulated by the pulse shaping filter gain. The pulse shaping filter has small ripples and 3 dB gain loss at the band-edge of the baseband. These peaks have powers that are lower than the TX-to-RX leakage power, however, still higher than the target return signal power. This is referred as amplitude distortion in [4]. More discussion is given in Annex A.

The following steps are applied to pick the desired tone:

1. The local peaks are sorted in a descending order based on their peak powers.

2. Only the top n_{tone} tones, other than the near DC spurs within the normalized frequency range of $[-0.005, 0.005]$, are picked into the selected set.

3. These selected tones are then assigned indices based on their coordinates on the frequency axis. The indexing starts at the DC, continues leftward to $-0.5f_B$, wraps-around at $0.5f_B$ (f_B is the baseband sampling frequency), then comes back leftward to DC. This is how we index these n_{tone} tones from 0 to $n_{spur} - 1$.

4. In our simulation model, only one selected tone is tracked to reduce the system complexity. The picked index is within the set of $\{0, \dots, n_{tone} - 1\}$. On the other hand, from the ECCM perspective, the more tones that can be tracked and the more sophisticated technique used for desired tone identification, the greater the counter jamming abilities.

4.12 Range estimation

Let S be the picked tone location from the sum-beam signal in the FFT domain of $[0, N_{FFT} - 1]$. The normalized quantity $\frac{(\mathrm{N_{FFT}-S})}{N_{FFT}}$ represents the normalized frequency distance between the tone location and DC, and it accounts for the round trip propagation delay based on the chirp signal characteristics. Therefore, the chirp signal characteristics described in the equation $\frac{(\mathrm{N_{FFT}-S})}{N_{FFT}} * f_B = 2b * 2\tau$ holds true, where τ is the one-way propagation delay in second. The target range is thus estimated based on the relative distance between the tone location and DC in the frequency domain:

$$R = \frac{(N_{FFT} - S) * c * f_B}{4bN_{FFT}}. \tag{30}$$

where c is the free space speed of light.

4.13 Indirectly velocity estimation

Based on two range and angle estimations in two N_{FFT}-point FFT windows separated by $N_{FFT} * dd$ samples at the baseband sampling rate f_B, we can estimate the velocity on x, y, z axis

$$v_x[u] = \frac{\mathrm{x}[u] - \mathrm{x}[u + dd]}{N_{FFT} * dd * T_B}$$

$$v_y[u] = \frac{\mathrm{y}[u] - \mathrm{y}[u + dd]}{N_{FFT} * dd * T_B} \tag{31}$$

$$v_z[u] = \frac{\mathrm{z}[u] - \mathrm{z}[u + dd]}{N_{FFT} * dd * T_B}$$

where u denotes the u^{th} FFT window, and

$$\mathrm{x}[u] = R[u] * \cos(\phi[u]) * \sin(\theta\,[u])$$

$$\mathrm{y}[u] = R[u] * \sin(\phi[u]) * \sin(\theta\,[u])$$

$$\mathrm{z[u]} = R[u] * \cos(\theta\,[u])$$

4.14 Peak value of the desired tone in other beams

Since the tone location S can be determined based on the sum-beam signal, we do not need to search for the desired tone locations for the signal from the lu, ld, ru, rd directions. The value of p_{pq} ($p = l\ or\ r, q = u\ or\ d$) is simply evaluated as:

$$p_{pq}(S) = 20\log_{10}\left(\left|\sum_{n=1}^{N_{FFT}} y_{pq}[n] e^{-\frac{2\pi jSn}{N_{FFT}}}\right|\right) \tag{32}$$

4.15 Time domain modelling via fractional delay filter

The round-trip time delay $\frac{2R(nT_S)}{c}$ consists of two parts, i.e., an integer delay part $\mathrm{round}\left(\frac{2R(nT_S)}{c}\right)$ and a fractional delay part τ_f within $[-0.5, 0.5]$ of T_s, where

$$\tau_f = \frac{2R(nT_S)}{c} - \mathrm{round}\left(\frac{2R(nT_S)}{c}\right) \tag{33}$$

A filter with the approximated all pass characteristics in the passband of $\left[-\frac{1}{2K}, \frac{1}{2K}\right]$ means that the fitter has unit gain and linear phase slope within $[-\pi, \pi]$ in its passband, where K is the oversampling factor. Using the filter in the oversampling domain, we can do interpolation to obtain the required signal phase. This technique is called Lagrange interpolation filter, which can be expressed as

$$h(n) = \prod_{k=0,k\neq n}^{P} \frac{D-k}{n-k}, \tag{34}$$

where $D = \tau_f + \text{floor}\left(\frac{P}{2}\right)$, where P is the order of the Lagrange filter. For example, when $K = 2$, the interpolation filter for a fractional delay of 0.25 has a gain and phase response as shown in Figure 10.

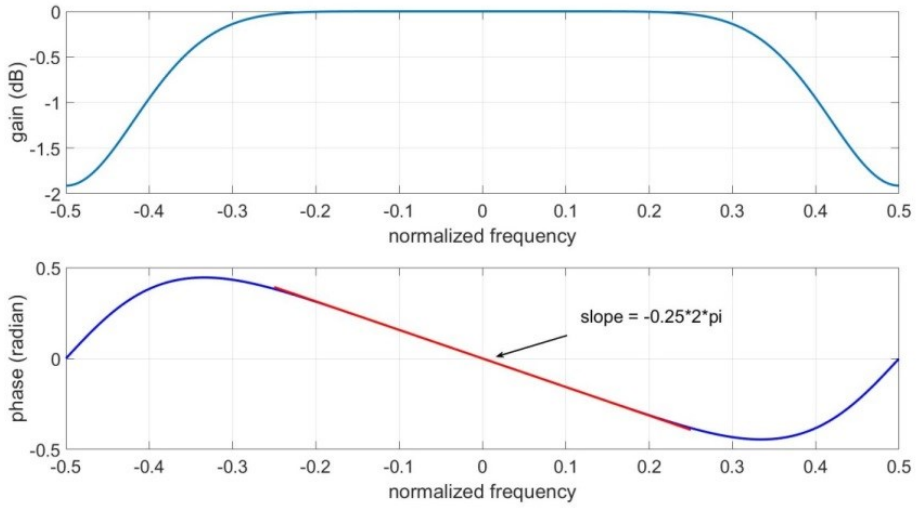

Figure 10: *Gain and phase response of a Lagrange filter of order 8 and delay = 0.25.*

5 RF specifications for simulations

5.1 Transmit and receive antenna patterns

The radar operates from 2.5 GHz – 3.5 GHz within S-band ($2-4\ GHz$), and the centre frequency of the radar is 3 GHz. Frequency agility within 2.5 GHz – 3.5 GHz is assumed. The TX-to-RX separation distance d_{TR} is 2.6 $meters$. We use microstrip patch antenna in this report. There is only one patch antenna at the TX, which forms a wide beam. There are an array of patch antennas at the RX. Recent work [8] justifies that microstrip patch antenna bandwidth can be improved to about 1 GHz using width extension and taper matching. Another reason of using patch antenna is that there is a closed form formula for simulating the patch antenna pattern. The coordinate system is shown in Figure 11.

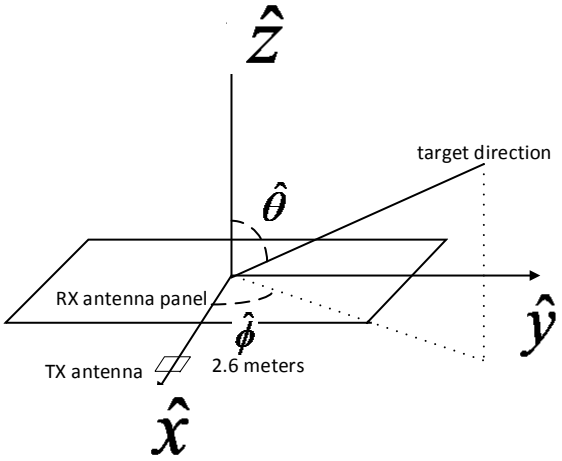

Figure 11: *The coordinate system of the receive patch antenna panel.*

The patch antenna pattern is given as follows [9]:

$$G_{rR}(\hat{\phi},\hat{\theta}) = 7 + 20\log_{10}\Big(\big(sinc(\pi W sin(\hat{\phi})\sin(\hat{\theta}))\cos(\pi L cos(\hat{\phi})\sin(\hat{\theta}))\big) + 10\log_{10}\Big(\cos(\hat{\phi})^2 + \big(\sin(\hat{\phi})\cos(\hat{\theta})\big)^2\Big)\Big), \tag{35}$$

where the mainlobe gain is assumed to be 7 dBi. The quantity W and L are width and length of the patch antenna respectively. For simplicity, we also assume that $G_{tR}(\hat{\phi},\hat{\theta}) = G_{rR}(\hat{\phi},\hat{\theta})$. In our simulation, W and L are both chosen to be $0.33 * \lambda\ at\ 3\ GHz\ =\ 3.3\ cm$.

5.2 Transmit-to-receive leakage power levels

With the $64x64$ receive array, the size of the array is $3.2\ m$ by $3.2\ m$ with the $0.05\ m$ antenna spacing. The TX antenna is located at $(0, \pi/2, 2.6)$ of the spherical coordinate $(\hat{\phi}, \hat{\theta}, \hat{R})$ shown in Figure 11. Ideally the TX-to-RX antenna gain is 0 in the linear scale. However, due to non-ideality of the antenna design, this gain is about $-20\ dB$ down from the mainlobe level [8]. The lowest free space propagation path loss at $1.05\ meters$ is about $41\ dB\ at\ 2.5\ GHz$ using the far field approximation. The highest free space propagation path loss at $4.15\ meters$ is about $56\ dB$ at $3.5\ GHz$. We assume that PA has a transmit power of $47\ dBm$, namely $50\ W$. The highest transmit-to-receive leakage power level is equal to $47 + 2 * (7 - 20) - 41 = -20\ dBm$. The lowest transmit-to-receive leakage power level is equal to $47 + 2 * (7 - 20) - 56 = -35\ dBm$. For simplicity, we just take the worst case scenario, and assume that it is $-20\ dBm$ for all receive antenna elements in the simulations. We set a fixed RF gain for each RF chain of each receive antenna.

5.3 RF gain and noise figure assumptions

With -20 dBm TX-to-RX leakage power and about 1 GHz bandwidth, the gain stage table is shown below (the sequence of the chain is from the left to the right):

Table 1: *RF gain and noise figure.*

	Band filter (2–4 GHz)	**LNA (2.5–3.5 GHz)**	**Filter0**	**LO Mixer (down to 1 GHz)**	**Filter1**	**IF amplifier**	**Filter2**	**COHO Mixer (down to 80 MHz I,Q)**	**Filter3**
Gain (dB)	-1	10	-1	-10	-1	24	-1	5	-1
Noise figure (dB)	1	3	1	10	1	5	1	10	1
Gain (linear)	0.79432823	10	0.79432823	0.1	0.7943282	251.18864	0.7943282	3.1622777	0.7943282
F (linear)	1.25892541	1.99526231	1.25892541	10	1.2589254	3.1622777	1.2589254	10	1.2589254
cascaded gain (linear)	0.79432823	7.94328235	6.30957344	0.6309573	0.5011872	125.89254	100	316.22777	251.18864
F (linear, Friis formula)	1.25892541	1.25296102	0.03259678	1.4264039	0.4103691	4.3143111	0.0020567	0.09	0.0008188
Cascaded F (linear)	1.25892541	2.51188643	2.54448321	3.9708871	4.3812562	8.6955673	8.6976241	8.7876241	8.7884428
Cascaded NF (dB)	1	4	4.05599589	5.9888754	6.4159865	9.3929792	9.3940063	9.4387147	9.4391193

Due to using $1\ GHz$ bandwidth, the LNA gain is lower than a narrow band LNA. The first stage mixer has a gain of $-10\ dB$ and contributes to a significant amount of the noise figure. Due to its low gain, it operates at much lower than the $1\ dB$ compression point and we can safely ignore the intermodulation level.

At the ADC input, the signal is amplified to $4\,dBm$, we assume a 16 bit ADC ($80\,MSPS$, pipepline ADC [11]) with $SFDR = 90\,dBc$ and maximum output $SNR = 80\,dB$. For $80\,MHz$ signal bandwidth, the noise at the antenna port is $-174 + 9.44 + 89 = -75.56\,dBm$. With $24\,dB$ gain, it becomes $-51.56\,dBm$ at the ADC input. We can assume the leakage signal is at $-6\,dBFS$ for the ADC input. In this case, the ADC introduced noise is only $-70\,dBm$. The input noise to ADC is $-51.5\,dBm$. For $BW = 40\,MHz$, this is exactly, $2x$ oversampling. For $BW = 10\,MHz$, this is $8x$ oversampling. With both computations, the noise figures are about $9.5\,dB$. In our simulations, we just assume $10\,dB$ noise figure as a ballpark number.

6 Simulation results

6.1 Simulink setup

Simulink modeling is conducted based on the mathematical models described in the previous sections. Simulink exactly mimics hardware processing. Corresponding modules of radar TX, radar RX, and over-the-air propagation are created in the Simulink environment. To simulate multiple target tracking, four targets are simulated. The parameter set can be found in the following table.

Table 2: *Simulation parameters.*

Variable name	Value	Remarks
N	64	Number of receive antenna elements on the z axis
M	64	Number of receive antenna elements on the x axis
h^c	exp(1i*rand(4,1))	Phases of the channel of the four target skin returns
(ϕ_0, θ_0)	$\left(\frac{\pi}{2}, \frac{\pi}{2}\right) radian$	The azimuth and elevation angle for the RX beam
$aa0$	$\phi_0 + (1 - 2 * rand(4,1)) * \frac{\pi}{4}$ $radian$	The initial azimuth angles of the four targets
$taa0$	$Round\left(aa0 * \frac{180}{\pi}\right) * \frac{180}{\pi}$ $radian$	The initial value of the azimuth tracking angle
$ae0$	$\theta_0 + \left(1 - 2 * rand(4,1)\right) * \frac{\pi}{8}$ $radian$	The initial elevation angles of the four targets
$tae0$	$Round\left(ae0 * \frac{180}{\pi}\right) * \frac{180}{\pi}$ $radian$	The initial value of the elevation tracking angle

Variable name	Value	Remarks
R_0	[3,7,11,15] km	The initial distances between the radar and the four targets
f_c	3 GHz	The carrier frequency of the radar and the jammer
f_B	variable	The baseband sampling rate
f_s	$2f_B$	Oversampling rate
v	[3349 1000 100; 2200 1000 100; 1200 800 200; 5000 2000 1000] km/h	Each row: velocity of each target towards the radar on x, y, z axis of the receiver coordinate system in Section 4.2
$accel$	[200 100 30; 200 100 30; 200 100 30; 1000 300 20] m/s^2	Each row: velocity acceleration of each target towards the radar on x, y, z axis of the receiver coordinate system in Section 4.2
b	10 GHz/s for 10 MHz BW 40 GHz/s for 40 MHz BW	Chirp signal slope
G_{rR}	According to Equation (35)	Radar RX antenna gain between radar RX antenna and the four targets
G_{tR}	the same as G_{rR}	Radar TX antenna gain between radar TX antenna and the four targets
σ	$17 * ones(4,1)$ dBm^2	RCS of the four targets
d_c/λ	0.5	the ratio of antenna spacing and wavelength
PtR	47 dBm	Radar transmit power

Variable name	Value	Remarks
$noise\_fl$	-164 dBm/Hz	Noise floor including the noise figure of 10 dB
$rrcord$	32	Root raised cosine pulse shaping filter order in the baseband sampling rate
$lagord$	8	Lagrange filter order in the oversampling domain.
$lpwr$	$-20\ dBm$	TX to RX leakage power for each receive antenna
N_{FFT}	variable	Number of FFT points
dd	variable	Delay of about 0.5 second
p_{prox}	16	The proximity range number for desired tone detection rule 1 in Section 4.11
c_1	0.044 for 3 km distance	The PI controller parameter, scaling with the distance
c_2	$1/64$	The PI controller parameter
n_{spur}	1	Select the strongest tone in the spectrum
$spurchoice$	0	Choose the 0th tone within the n_{tone} tone set

To illustrate the range resolution and time-bandwidth product effects, two scenarios are studied in this report.

1. Baseband sampling rate $f_B = 10\ MHz$, sweep time $= 0.8192\ ms$, $N_{FFT} = 8{,}192$.
2. Baseband sampling rate $f_B = 40\ MHz$, sweep time $= 1.6384\ ms$, $N_{FFT} = 65{,}536$.

For case 1, the range resolution is $\frac{c*f_B}{4bN_{FFT}} = \frac{c*10\ MHz}{4*10\ GHz/s*8192} = 9.16\ m$. The time-bandwidth product is 8,192. The maximum unwrapped range is $75\ km$.

For case 2, the range resolution is $\frac{c*40MHz}{40\ GHz/s*4*65536} = 1.14\ m$. The time-bandwidth product is 65,536. The maximum unwrapped range is still $75\ km$.

Since case 2 and case 1 uses the same PA level, case 2 has 6 dB lower RF SNR than that of case 1. However, the time-bandwidth product of case 2 is 9 dB higher than case 1. Therefore, the SNR gain after FFT of case 2 *vs* case 1 is 3 dB corresponding to the difference of time-bandwidth product and RF SNR in dB.

The angle tracking starts at the initial tracking angles $(taa0, tae0)$ and intend to track the true (ϕ, θ).

Note that in this simulation, only the strongest tone in the spectrum is chosen. This implies that for a narrow RX beam, only one target with the strongest skin return is tracked. If a narrow RX beam covers multiple targets, we need to use time-division-multiplexing processing to sequentially detect the propagation delay of each target. This part will be deferred to future work.

6.2 Effects of windowing and notch filter

Due to the continuous beamforming angle update, the DC value after the digital beamforming varies over time. This causes significantly high sidelobes near DC as shown in Figure 12 because the DC value by itself is very strong. With a Chebyshev window and notch filter, we successfully tackle this effect as shown in Figure 13 and Figure 14. Using a notch filter knocks down the DC spur and makes the desired tone selection rule easier to apply when the desired tone is rather close to DC.

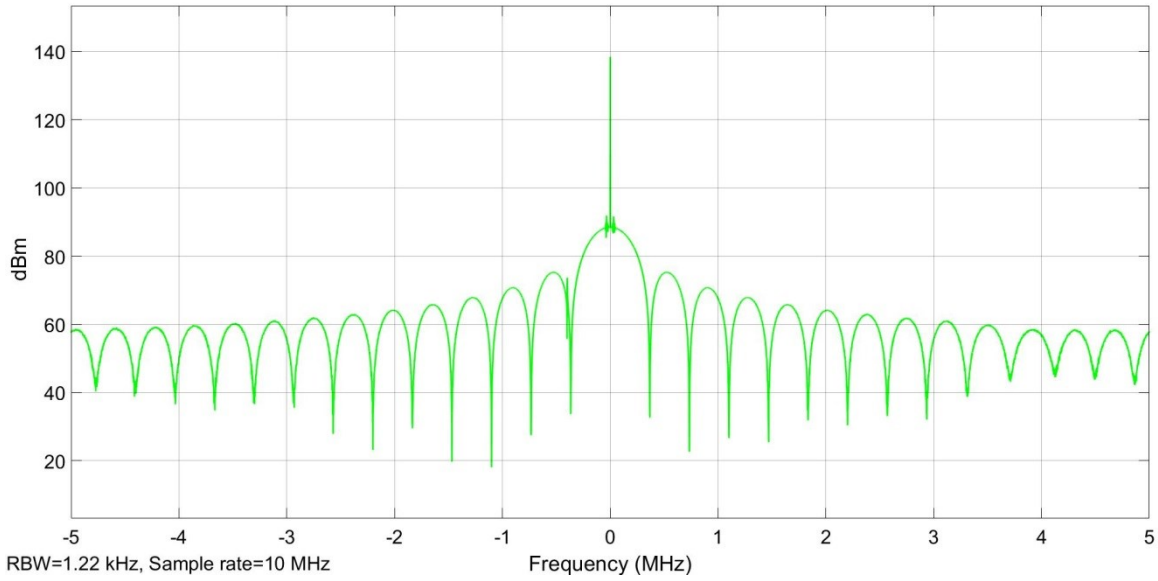

Figure 12: *Spectrum plots for the target 0 for case 1 with no notch filter and no FFT window function at the start of simulation.*

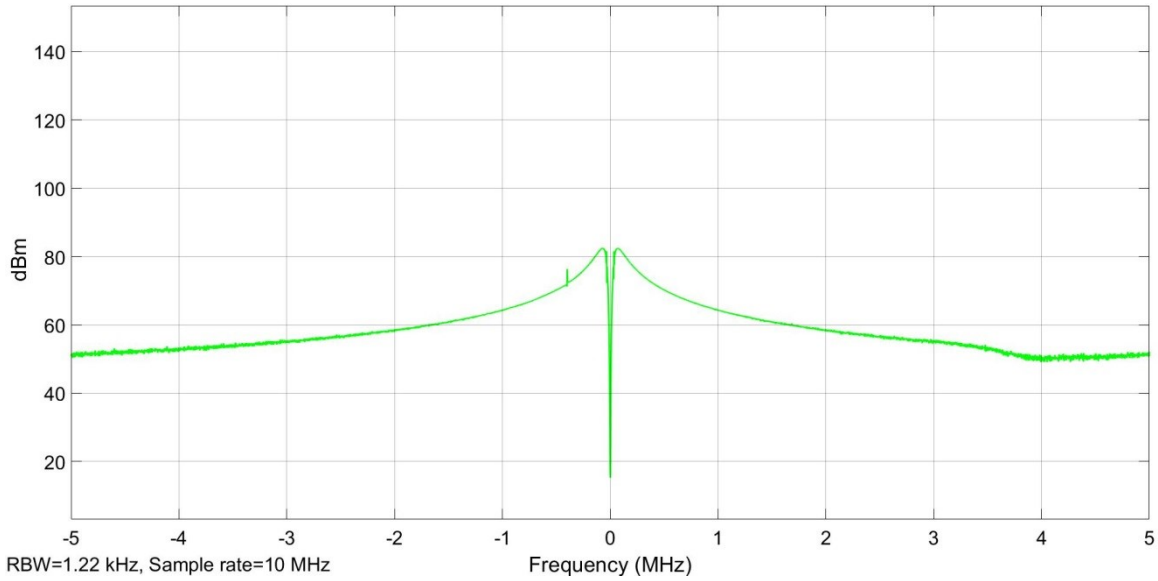

Figure 13: *Spectrum plots for the target 0 for case 1 with notch filter and no FFT window function at the start of the simulation.*

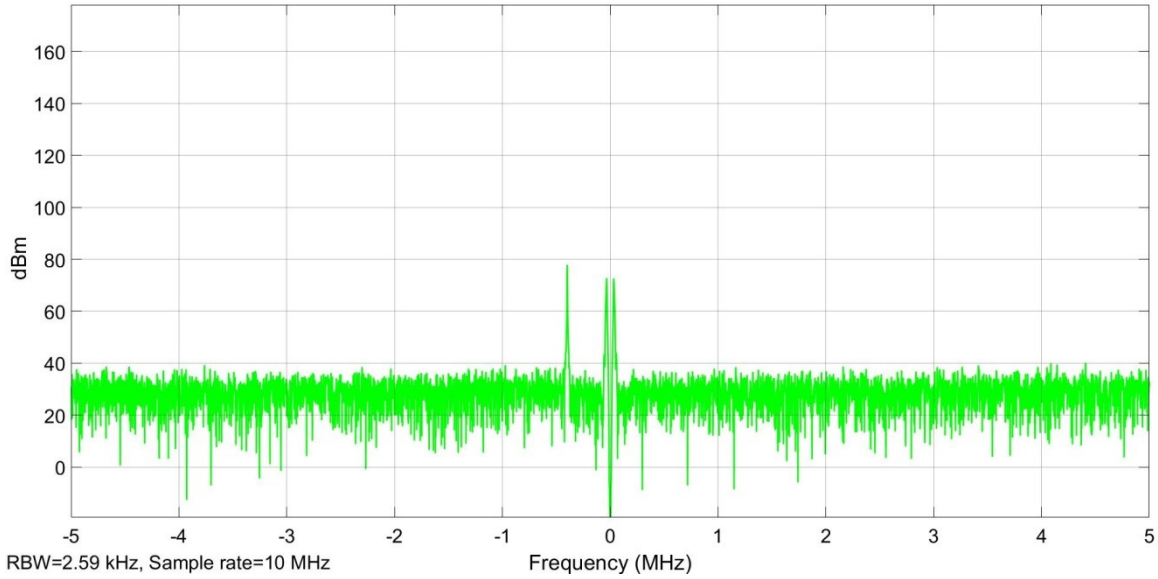

Figure 14: *Spectrum plots for the target 0 for case 1 with both notch filter and Chebyshev window at the start of the simulation.*

6.3 Spectrum plot after the notch filter for $f_B = 10\ MHz$

The simulation run time is 1 second. When the target tracking process finishes, we plot the spectrum after the notch filter as in Figure 15. Since the beams formed by 64×64 antenna array is very narrow, each spectrum plot only sees three peaks: the target tone using the beam formed based on the target tracking angle and two near DC spurs. The closer the distance of the target, the stronger the tone strength.

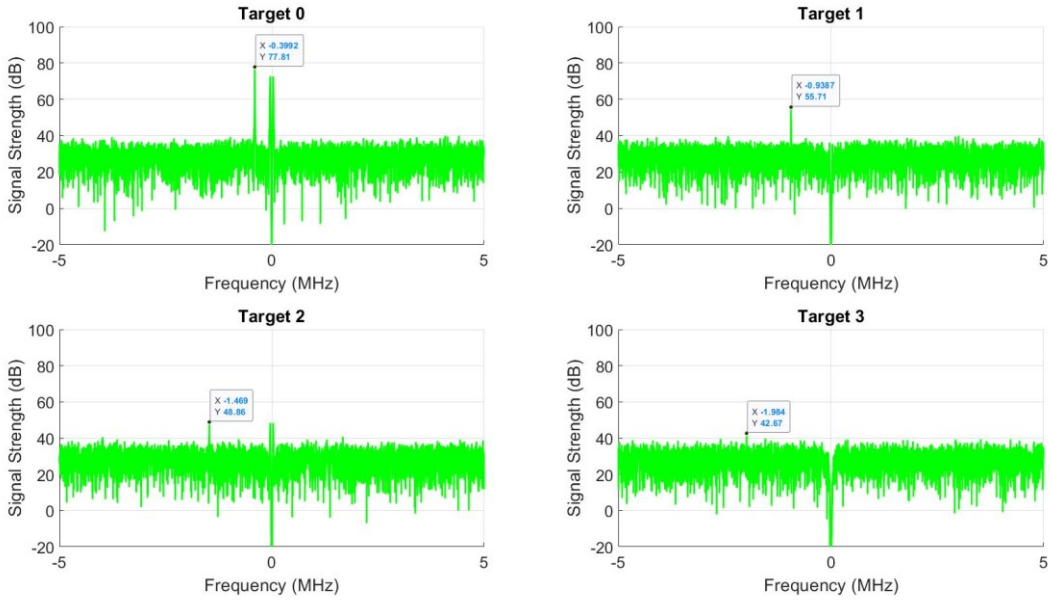

Figure 15: *Spectrum plots for the targets for case 1.*

6.4 Range tracking results for $f_B = 10\ MHz$

We illustrate the range tracking in Figure 16. The range estimation closely follows the true range of each target. At the 15 km range, the range estimation has sporadic errors because the spurs caused by the white Gaussian noise are occasionally stronger than the desired tone energy.

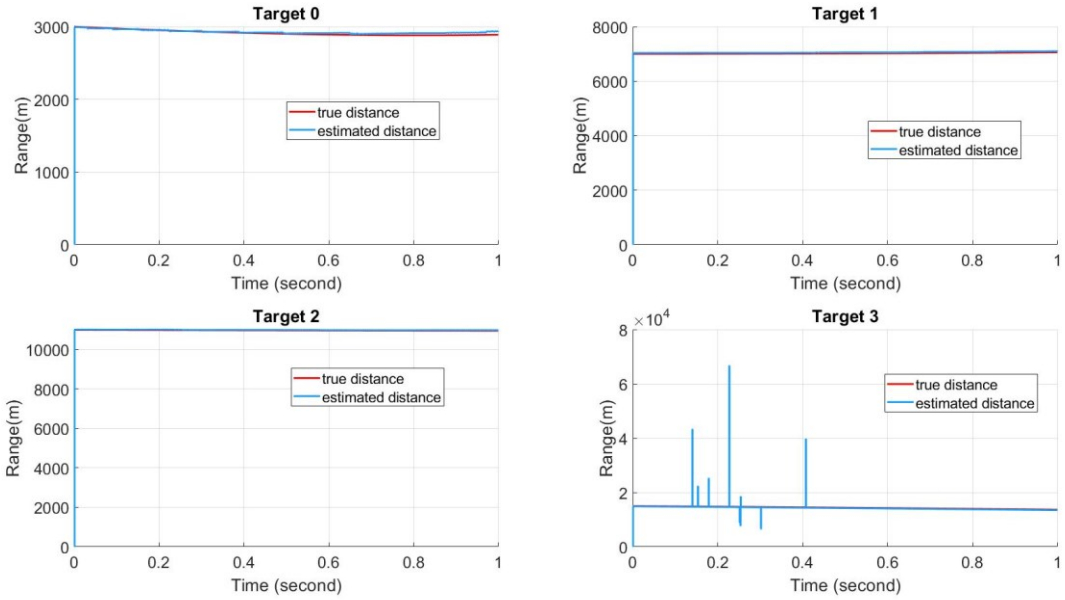

Figure 16: *Range estimation for the targets for case 1.*

6.5 Angle tracking results for $f_B = 10\ MHz$

We illustrate angle tracking in Figure 17. Clearly, our angle tracking closely follows the target movement.

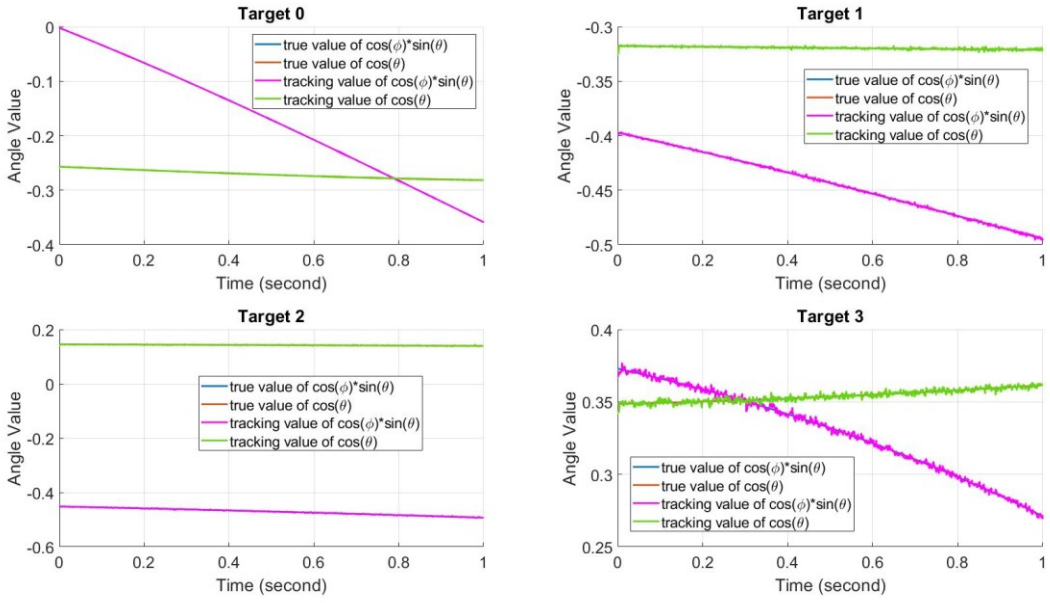

Figure 17: *Angle tracking for the targets for case 1.*

6.6 Velocity tracking results for $f_B = 10\,MHz$

We illustrate the velocity tracking in Figure 18. The tracking results are good for 0.5 second of delay in Equation (31).

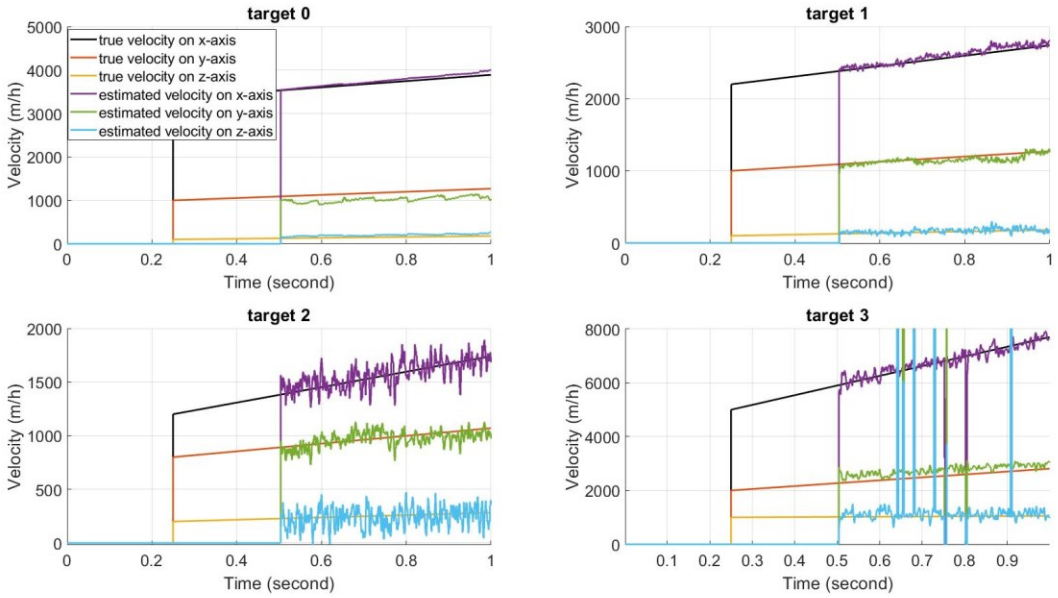

Figure 18: *Velocity tracking for the targets for case 1.*

6.7 Spectrum plot after the notch filter for $f_B = 40\,MHz$

Similarly, we plot the spectrum after the notch filter for $f_B = 40\,MHz$ in Figure 19. Comparing with $f_B = 10\,MHz$, the noise floor is about $9\,dB$ lower because of using the spectrum normalization factor $= N_{FFT}$. The SNR (signal power to noise power) improvement is $0 - 4\,dB$ by comparing the desired tone power values at the markers in Figure 15 and Figure 19.

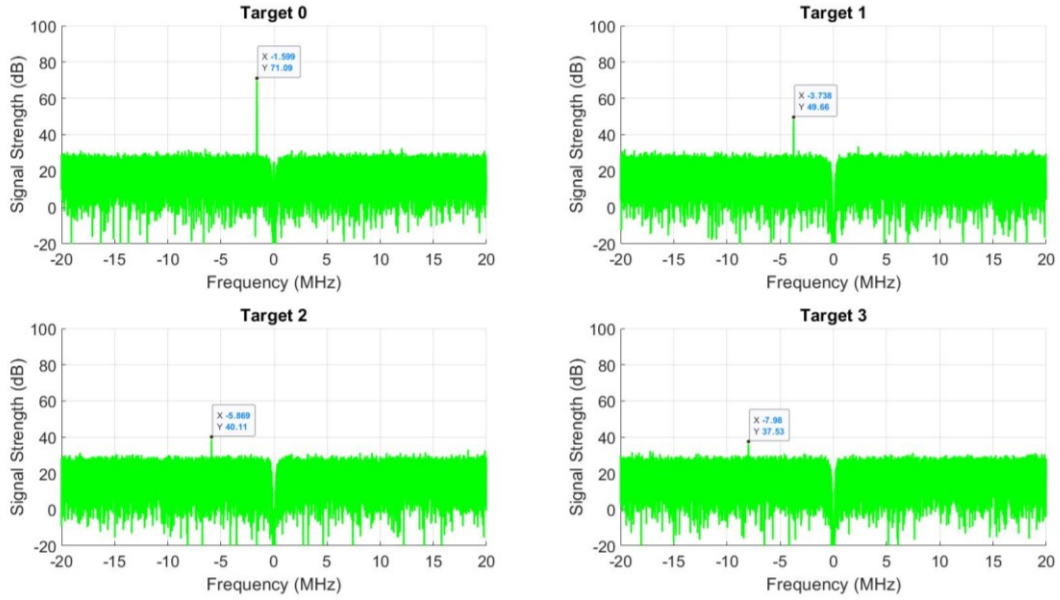

Figure 19: *Spectrum plots for the targets for case 2.*

6.8 Range tracking results for $f_B = 40\ MHz$

We illustrate the range tracking in Figure 20. The range estimation closely follows the true range of each target.

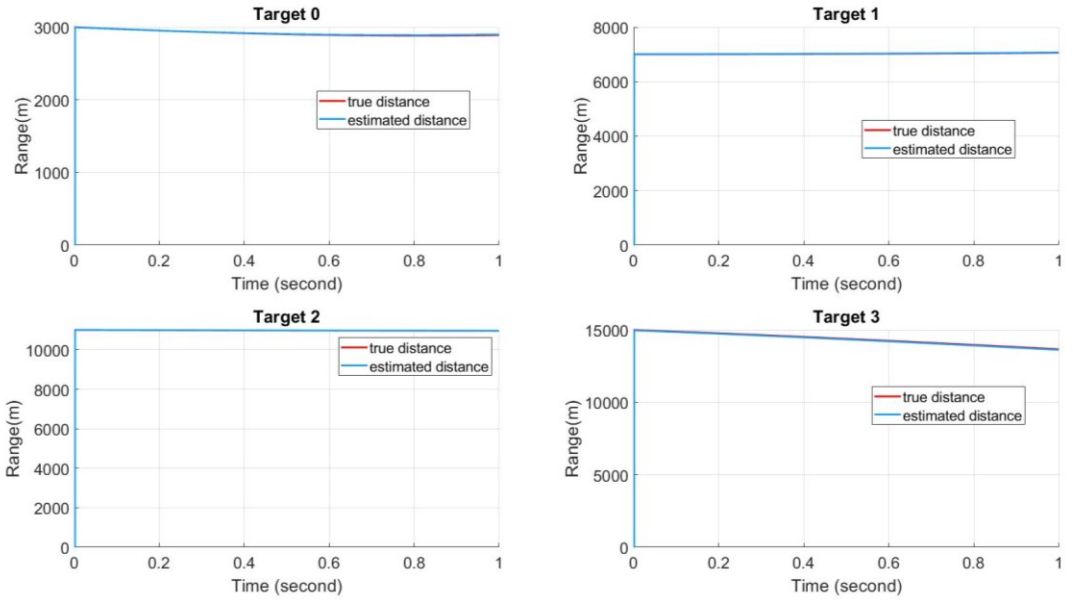

Figure 20: *Range estimation for the targets for case 2.*

6.9 Angle tracking results for $f_B = 40\ MHz$

Angle tracking results are illustrated in Figure 21. Clearly, our angle tracking follows closely the target movement.

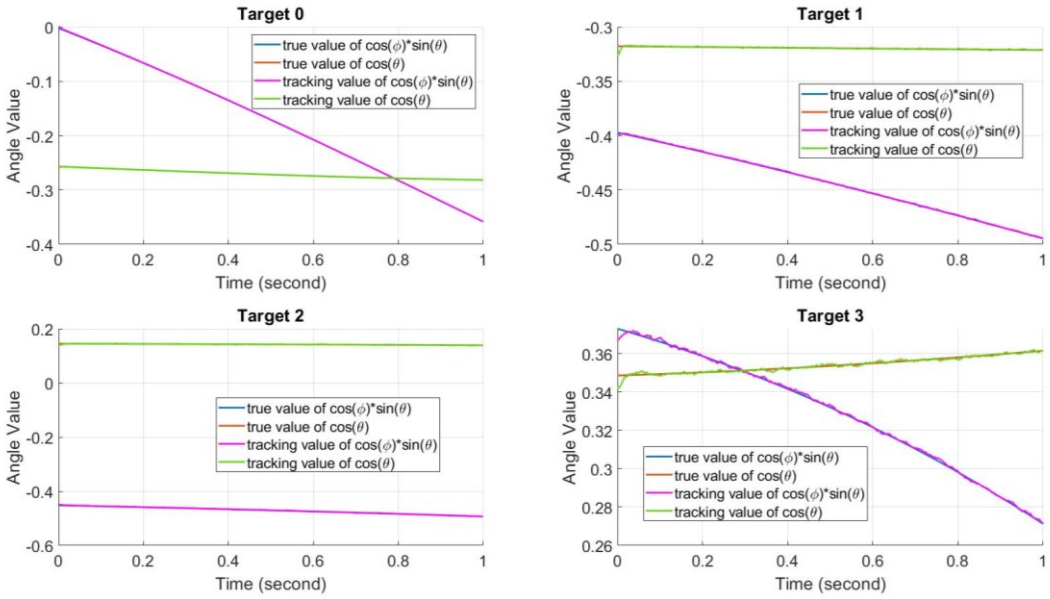

Figure 21: *Angle tracking for the targets for case 2.*

6.10 Velocity tracking results for $f_B = 40\ MHz$

We illustrate the velocity tracking in Figure 22. The tracking results are good for 0.5 second of delay in Equation (31).

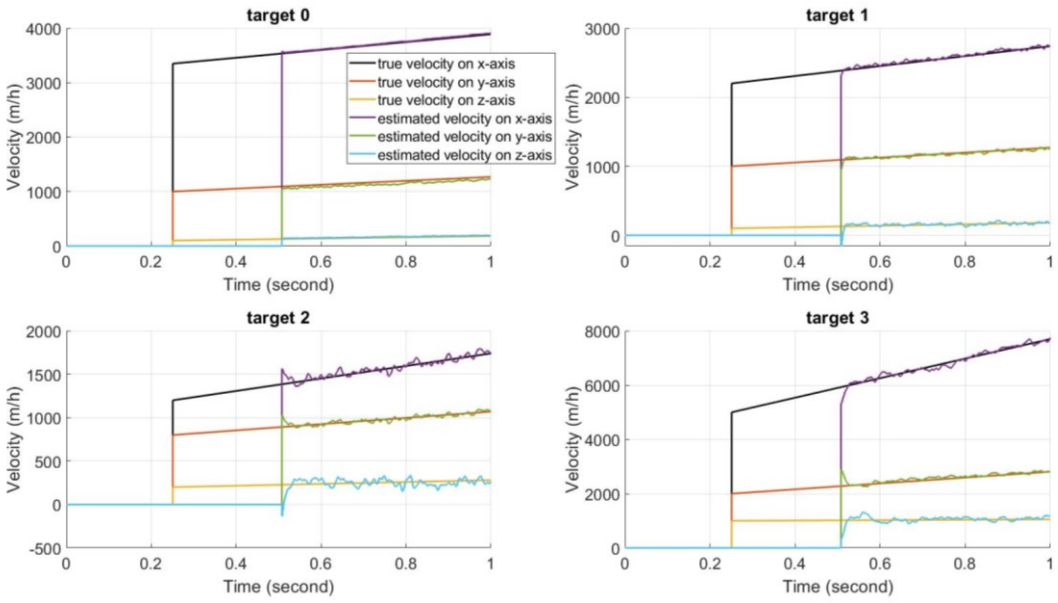

Figure 22: *Velocity tracking for the targets for case 2.*

6.11 Simulation summary

From the simulation results, we conclude that the proposed angle tracking algorithm is robust enough to track the angle of arrival of the targets. The DPA radar can perform multiple target tracking. Note that our proposed velocity tracking is derived from angle and range tracking results. This estimation method is different from estimating Doppler directly for pulse-doppler radars. The range and Doppler dilemma [10] does not apply to our case.

7 Conclusion

In this Scientific Report, a digital beamforming technique based on coherent array combining and FFT processing is proposed for FMCW digital phased array radars. This frequency domain technique reduces the complexity of the time domain convolution approach by using FFT. It also enables the separation of target skin return tone and TX-to-RX leakage spurs. We found that the strong DC spur has significantly high sidelobes caused by continuous digital beamforming. By applying a Chebyshev window function, the sidelobes of the DC spur are effectively suppressed. An angle tracking method is proposed which relies on the post-FFT tone energy. This is not exactly the matched filter response (The exact matched filter response requires finer estimation of the offset frequency). However, it has enough information for angle tracking. PI controller is used to stabilize the angle tracking process. The future work is to prototype an emulation system in FPGA using the Simulink to FPGA design methodology.

References

[1] A. G. Stove, A. L. Hume and C. J. Baker, "Low Probability of Intercept Radar Strategies," *IEE Proceeding, Radar, Sonar and Navigation*, Vol. 151, Issue 5, pp. 249–260, Oct. 2004.

[2] D. Adamy, EW 101, A First Course in Electronic Warfare, Artech House, 2001.

[3] C. A. Davila, G. D. Hopkins, D. D. Aalfs and F. Wright, Modeling and Simulation of RF Electronic Warfare Systems, Georgia Tech Professional Education Training Material, 2013.

[4] A. G. Stove, "Linear FMCW Radar Techniques," *IEE proceedings, Vol. 139, No. 5,* Oct. 1992,

[5] L. B. Van Brunt, Applied ECM, EW Engineering, Inc., 1978.

[6] D. Johnson and G. Brooker, "Research Radar for Unmanned Navigation," *2008 International Conference on Radar*, pp. 160–170.

[7] M. Jain, J. I. Choi, T. M. Kim, D. Bharadia, S. Seth, K. Srinivasan, P. Levis, S. Katti and P. Sinha, "Practical, Real-time, Full Duplex Wireless," *2011 MobiCom Conference*.

[8] M. S. Rabbani and H. Ghafouri-Shiraz, "Simple Method for Enhancing Bandwidth of a Rectangular Microstrip Patch Antenna," *2nd IET Annual Active and Passive RF Devices Seminar*, Oct. 2014.

[9] K. R. Carver and J. W. Mink, "Microstrip Antenna Technology," *IEE Trans. on Antennas and Propagation*, *Vol. AP-29, No. 1*, Jan. 1981.

[10] N. Filippo, Introduction to Electronic Defense Systems, second edition, Artech House, 2011.

[11] Analog Devices Inc., AD9446, 16-Bit, 80/100 MSPS ADC, Data Sheet.

Annex A Passing the chirp signal through a low-pass filter

The chirp signal can be synthesized in the digital domain. Then it needs to be up-converted to RF at the radar transmitter. The up-conversion process requires low pass filtering. If the gain of the low pass filter is not flat in the chirp baseband $[-\frac{f_B}{2}, \frac{f_B}{2}]$, the chirp signal's amplitude can be modulated by the gain of the filter when the chirp signal sweeps across the pass-band of the low pass filter.

Since we use root-raised-cosine (RRC) filter for pulse-shaping, it is symmetric around DC in the spectrum. Assuming that the chirp rate is b Hz/s, the amplitude change of the chirp signal is periodic with a period of $\frac{f_B/2}{b}$. The frequency of the amplitude change is $\frac{2b}{f_B}$. For $= 10\ GHz/s$, $f_B = 10\,MHz$, the frequency of the amplitude change is $2\ kHz$. This will be the lowest frequency component of the near DC spurs.

The ripples in the pass-band have a period of 0.3125 MHz in the frequency domain. Thus the gain variation caused by the ripples has a time period of $0.3125\ MHz/10\ GHz/s\ = 3.125e-5\ second$. The gain change frequency is therefore about $32\ KHz$, corresponding to the strongest near DC spur shown in Figure A.1. The rest of the harmonics spread apart every 2 kHz.

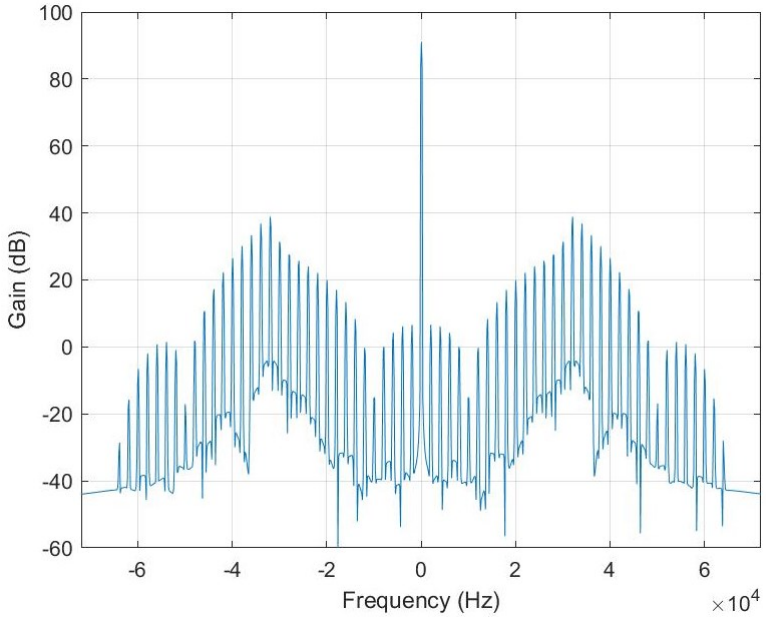

Figure A.1: *Amplitude modulation effect of the chirp signal after de-chirping.*

Annex B Notch filter design

Using a DC notch filter eases the job of desired tone identification for the near DC tones. The notch filter can be a simple first order IIR filter as the following:

$$H(z) = \frac{1 - z^{-1}}{1 - 0.975z^{-1}} \tag{B.1}$$

Since we want to increase the gain slope of the DC null, we can use a high order IIR filter. This gives multiple times as big of the slope value as the first order IIR. In our design, the 4th order IIR filter rejects the DC and suppress the near DC components:

$$H(z) = \frac{(1 - z^{-1})^4}{(1 - 0.975z^{-1})^4} \tag{B.2}$$

This filter can cancel the DC frequency component by more than 80 dB, and has less than 10 dB gain reduction when the normalized frequency is bigger than 0.005.

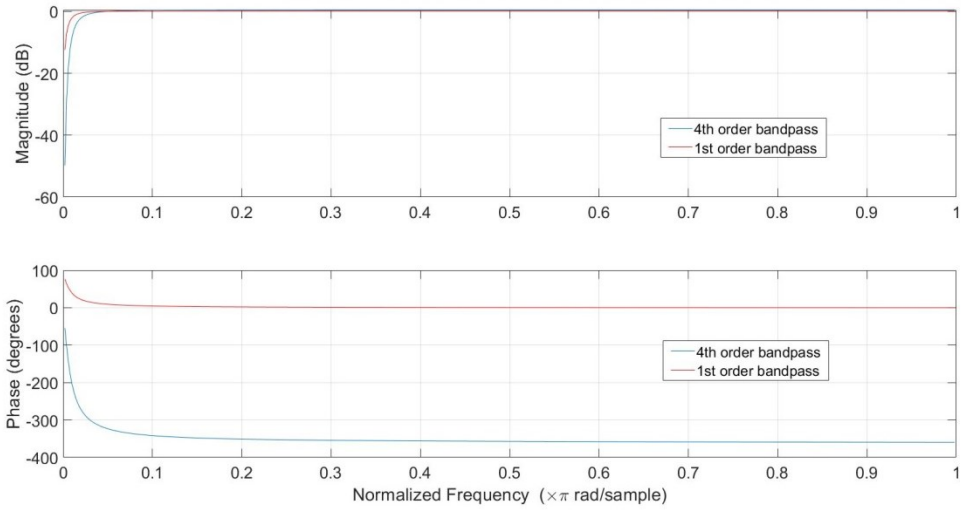

Figure B.1: *Gain and phase responses of the notch filters.*

List of symbols/abbreviations/acronyms/initialisms

ADC	Analog to Digital Converter
AF	Array Factor
ASV	Array Steering Vector
AWGN	Additive White Gaussian Noise
Az	Azimuth angle
BB	Base-band
DBF	Digital Beamforming
DPA	Digital Phased Array
DRDC	Defence Research and Development Canada
DSP	Digital Signal Processing
ECCM	Electronic Counter-Countermeasures
ECM	Electronic Countermeasures
El	Elevation angle
EM	Electromagnetic
ESM	Electronic Support Measures
FMCW	Frequency Modulated Continuous Wave
FPGA	Field Programmable Gate Array
HWIL	Hardware-in-the-Loop
I/Q	In- and Quadrature-components
LPI	Low Probability Intercept
M&S	Modeling and Simulation
PA	Power Amplifier
R&D	Research and Development
RCS	Radar Cross Section
REW	Radar Electronic Warfare
RF	Radio Frequency
RRC	Root-raised-cosine
RX	Receiver
TTR	Target Tracking Radar
TX	Transmitter

DOCUMENT CONTROL DATA

*Security markings for the title, authors, abstract and keywords must be entered when the document is sensitive

1. ORIGINATOR (Name and address of the organization preparing the document. A DRDC Centre sponsoring a contractor's report, or tasking agency, is entered in Section 8.)

DRDC – Ottawa Research Centre
Defence Research and Development Canada, Shirley's Bay
3701 Carling Avenue
Ottawa, Ontario K1A 0Z4
Canada

2a. SECURITY MARKING (Overall security marking of the document including special supplemental markings if applicable.)

CAN UNCLASSIFIED

2b. CONTROLLED GOODS

NON-CONTROLLED GOODS
DMC A

3. TITLE (The document title and sub-title as indicated on the title page.)

Design of new Frequency Modulated Continuous Wave (FMCW) target tracking radar with digital beamforming tracking: A Scientific Report on high fidelity radar electronic warfare modelling and simulation and hardware in-the-loop

4. AUTHORS (Last name, followed by initials – ranks, titles, etc., not to be used)

Tang, T.; Wu, C.

5. DATE OF PUBLICATION (Month and year of publication of document.)	6a. NO. OF PAGES (Total pages, including Annexes, excluding DCD, covering and verso pages.)	6b. NO. OF REFS (Total references cited.)
December 2019	45	11

7. DOCUMENT CATEGORY (e.g., Scientific Report, Contract Report, Scientific Letter.)

Scientific Report

8. SPONSORING CENTRE (The name and address of the department project office or laboratory sponsoring the research and development.)

DRDC – Ottawa Research Centre
Defence Research and Development Canada, Shirley's Bay
3701 Carling Avenue
Ottawa, Ontario K1A 0Z4
Canada

9a. PROJECT OR GRANT NO. (If appropriate, the applicable research and development project or grant number under which the document was written. Please specify whether project or grant.)	9b. CONTRACT NO. (If appropriate, the applicable number under which the document was written.)
03dc - RF Warfare	

10a. DRDC PUBLICATION NUMBER (The official document number by which the document is identified by the originating activity. This number must be unique to this document.)	10b. OTHER DOCUMENT NO(s). (Any other numbers which may be assigned this document either by the originator or by the sponsor.)
DRDC-RDDC-2019-R175	

11a. FUTURE DISTRIBUTION WITHIN CANADA (Approval for further dissemination of the document. Security classification must also be considered.)

Public release

11b. FUTURE DISTRIBUTION OUTSIDE CANADA (Approval for further dissemination of the document. Security classification must also be considered.)

12. KEYWORDS, DESCRIPTORS or IDENTIFIERS (Use semi-colon as a delimiter.)

Beamforming; Radar Signal Processing; Detection and Target Tracking

13. ABSTRACT (When available in the document, the French version of the abstract must be included here.)

Frequency modulated continuous wave (FMCW) radars have large time-bandwidth product factor with long detection range and accurate range resolution using low emitting power, which impose a great challenge for electronic support measure (ESM) systems to detect such radars. For better understanding of the radar technology and assisting radar electronic warfare (REW) research and development (R&D), this Scientific Report presents a new FMCW radar system design with a phased array and digital beamforming (DBF) for monopulse multi-target tracking. The radar computer model can also be used in radio frequency (RF) high-fidelity modelling and simulation (M&S) for REW studies. A number of design challenges are addressed in the report, including the use of 1) Chebyshev window and digital notch filter to overcome the transmitter-to-receiver leakage in the radar, 2) DBF for simultaneously multi-target tracking, and 3) feedback control loop design. Using a digital filter, this report also introduces a new RF M&S scheme that addresses the continuous target movement modeled in the sampled signal domain. This scheme provides a general approach that allows the digital/time-based RF M&S to incorporate the analog signals at any required time instant without increasing the time sampling rate.

Les radars à onde continue modulée en fréquence (OCMF) ont un facteur produit durée-bande passante élevé, une grande portée de détection et une résolution en portée précise, malgré leur faible puissance d'émission. Cela complique grandement la détection par les systèmes de mesure de soutien électronique (MSE). Dans le but de mieux comprendre cette technologie radar et de soutenir les efforts de recherche et développement (R&D) en guerre électronique par radar (GER), le présent rapport scientifique contient la description d'un nouveau concept de système radar OCMF à balayage électronique et mise en forme numérique du faisceau pour la poursuite multicibles monoimpulsion. Le modèle informatique de radar présenté peut aussi servir en modélisation et simulation RF à haute fidélité pour les recherches en GER. Le rapport traite d'un certain nombre de difficultés de conception rencontrées, notamment l'utilisation 1) de la fenêtre de Tchébychev et d'un filtre numérique à coupure brusque pour éviter les pertes à la terre entre l'émetteur et le récepteur du radar; 2) de mise en forme numérique du faisceau pour la poursuite multicibles; et 3) d'une conception fondée sur une boucle de réaction. Le rapport présente aussi une nouvelle méthode de modélisation et simulation RF par filtrage numérique qui tient compte du mouvement continu des cibles modélisé dans le domaine des signaux échantillonnés. Il s'agit d'une technique générale qui permet à la modélisation et la simulation RF (temporelle ou numérique) d'intégrer des signaux analogiques au moment voulu sans devoir augmenter le taux d'échantillonnage.